

Design and Implementation of a Stewart Platform for Enhanced Patient Comfort in Ambulance Stretchers.

V.Naresh¹, Y.Santhosh kumar², L.Indirakumar³.

¹*Associate Professor, Department of Mechanical Engineering, Bharathidasan Engineering College, Natrampalli, Tirupattur District, TamilNadu state, India (Affiliated to Anna University, Chennai, TamilNadu, India).*

²*PG Student, Department of Mechanical Engineering, Bharathidasan Engineering College, Natrampalli, Tirupattur District, TamilNadu state, India (Affiliated to Anna University, Chennai, TamilNadu, India).*

³*Assistant Professor, Department of Mechanical Engineering, Bharathidasan Engineering College, Natrampalli, Tirupattur District, TamilNadu state, India (Affiliated to Anna University, Chennai, TamilNadu, India).*

Corresponding Author:-

Dr.V.Naresh

Associate Professor, Department of Mechanical Engineering, Bharathidasan Engineering College, Natrampalli, Tirupattur District, TamilNadu state, India (Affiliated to Anna University, Chennai, TamilNadu, India).

Mail id - nareshmeed@gmail.com

Abstract

In modern emergency medical services, patient safety and comfort during transportation are critical concerns. This paper presents the design and implementation of a Stewart Platform integrated into ambulance stretchers to enhance patient comfort by minimizing vibrations and sudden movements. The Stewart Platform, a type of parallel manipulator with six degrees of freedom, is utilized for its high precision and stability in motion control applications. The study explores the mechanical design, kinematic modeling, and control system integration required to implement the Stewart Platform in the stretcher framework. Key components include actuators, sensors, and a real-time microcontroller to enable adaptive damping and vibration isolation. Advanced control algorithms, including Proportional-Integral-Derivative (PID) and Model Predictive Control (MPC), are employed to dynamically adjust the platform's position and orientation in response to road conditions. Experimental results demonstrate the effectiveness of the system in reducing vibrations and tilt angles during simulated ambulance rides. The platform maintains stability within ± 2 degrees of tilt and reduces vertical oscillations by up to 70%. These improvements significantly enhance patient comfort and safety compared to conventional stretchers. This research contributes to the field of biomechanical engineering and emergency medical technology by providing a novel solution for mitigating transport-induced discomfort and potential injuries. Future work will focus on further miniaturization, cost optimization, and integration with telemedicine technologies to monitor and manage patient vitals during transit.

Keywords: Stewart Platform, Ambulance Stretcher, Vibration Isolation, Patient Comfort, Motion Control, Emergency Medical Services

1. INTRODUCTION

Ambulance transportation plays a critical role in pre-hospital emergency care, ensuring that patients receive timely medical attention. However, road conditions, abrupt vehicle movements, and vibrations often compromise patient comfort and safety during transit. These mechanical disturbances can exacerbate injuries, induce pain, and increase physiological stress, especially for patients with severe trauma or spinal cord injuries. Addressing these challenges necessitates innovative solutions to improve patient stability and comfort.

The Stewart platform, a parallel manipulator originally developed for flight simulators and industrial applications, has emerged as a promising technology for vibration isolation and motion compensation. Its six degrees of freedom (DOF) allow precise control over translations and rotations, making it highly adaptable for dynamic stabilization tasks. Recent

advancements in mechatronics and control systems have extended its applicability to the medical field, particularly in surgical platforms and rehabilitation devices.

This study explores the design and implementation of a Stewart platform integrated into ambulance stretchers to mitigate the impact of road-induced vibrations and improve patient comfort during transit. The system employs sensors and actuators to detect and counteract undesirable movements in real time, providing an adaptive stabilization mechanism. Conventional ambulance stretchers lack the ability to dynamically stabilize and isolate patients from road-induced disturbances, leading to discomfort and potential exacerbation of injuries. An effective vibration isolation system is essential to enhance patient safety and comfort. To design a Stewart platform capable of providing six DOF motion control for vibration isolation. To develop a control system for real-time monitoring and compensation of disturbances. To integrate the Stewart platform

with standard ambulance stretchers while ensuring portability and usability. To evaluate the performance of the system in reducing vibrations and improving patient comfort.

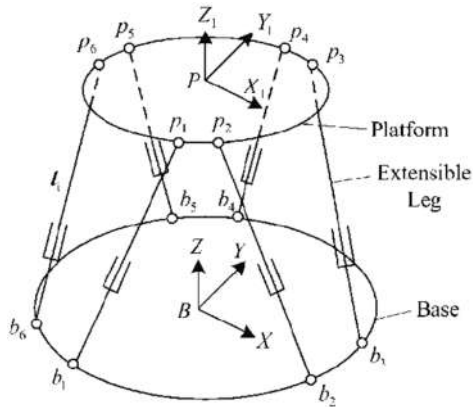
This research focuses on the mechanical design, actuation, and control systems required for the Stewart platform. It also includes simulations and experimental validations under controlled and real-world conditions. The study does not address medical diagnostics but aims to complement existing medical care by improving the patient transport experience.

Improving patient comfort during ambulance transportation can lead to better health outcomes and reduced stress levels. By leveraging the Stewart platform's capabilities, this project aims to set a new standard in emergency medical services, combining advanced engineering with patient care. Additionally, the findings may inspire further innovations in healthcare-related transportation and stabilization systems.

2. THE STEWART-PLATFORM BASED ROBOTIC WRIST

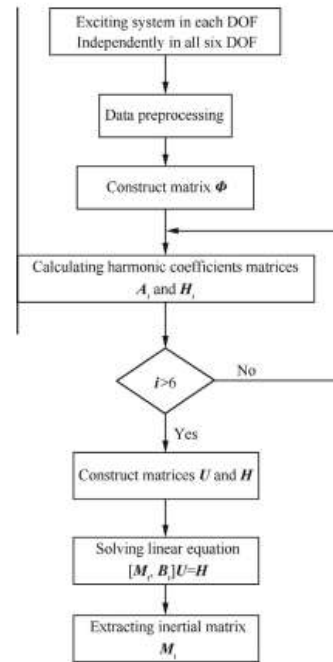
presents a robot manipulator of the Intelligent Robotic Laboratory (IRL) at the Goddard Space Flight Center (NASA), which consists of a 6 DOF Cincinnati T3 robot and a 6 DOF Stewart Platform-based robotic wrist mounted to the last link of the T3 robot. The manipulator has a total of 11 DOFs since 1 DOF of the wrist is identical to that of the T3 robot. The main function of the T3 robot is to perform gross motion, for example to bring the robotic wrist into its workspace and then let the wrist carry out fine motion required for high-precision operations such as assembly of parts, mating connectors, etc. As shown in Fig. 2, the design of the robotic wrist is based on the mechanism of the Stewart Platform. It

mainly consists of a payload platform, a base platform, six linear actuators and a gripper attached to the payload platform. The payload platform is coupled with the base platform by the actuators each of which is composed of a NSK ballscrew assembly mounted axially with a PMI d.c. motor. The motors drive the ballscrews to extend or shorten the actuator lengths whose variations will in turn produce the motion of the payload platform relative to the base platform. The actuator lengths are measured by six BALLUFF linear displacement transducers (LDT) mounted along the actuators. Forces/torques exerted by the gripper are acquired through a JR 3 Universal Force-Moment Sensor System mounted between the gripper base and the payload platform. Each end of the actuator links is mounted to the platforms by 2 DOF universal joints. The LDT signals are sent to the IRL local area network (LAN) via an ethernet board and a data translation input board resided in a PC/386. An Apollo workstation will take the sensor signals off the LAN by means of another ethernet board, performs all necessary computations for the implementation of control schemes, coordinate transformations, etc., and sends the actuating signals to the PMI motor drives via a data translation output board.



3. Identification process

The above analysis of the identification principle based on sinusoidal vibrations provides a solid foundation for a novel identification process. The steps of the identification approach are summarized as follows: (a) Excite the system in each of the six DOFs independently. In this step, the test frequency of the ground harmonic x_t should be chosen below the lowest open loop 'rigid' eigen frequency to avoid exciting relevant parasitic flexible modes of the system. Amplitudes of required harmonic reference signals should be chosen properly to minimize nonlinear effects caused by s_x and to moderate the exciting energy used for identification. (b) Preprocess data. The platform position S_{pi} is obtained using the forward kinematics solution and length signals of measurement actuators l_i . The platform force in the task space S_{fi} is calculated as $F = \frac{1}{4} J^T l \ddot{s}_x \bar{p}_{fai}$, where f_{ai} is the force signals of the measurement actuator.



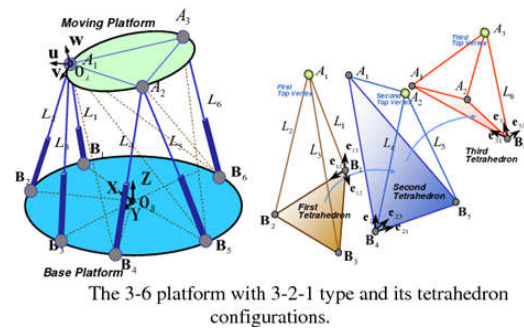
Flowchart of identification approach.

Method A

In the case of employing Method A, the maximum identified error is the difference between I_{xx} and I_{yy} , which is $3.4 \text{ kg}\cdot\text{m}^2$ and almost equal to the difference in the case of employing Method B ($3.0 \text{ kg}\cdot\text{m}^2$). Comparing with the inertial matrix identified using the nonlinear friction simulation model, it is found that the changing trends of the two inertial matrices are similar; e.g., the cross terms ($M_t(1,5)$, $M_t(2,4)$, $M_t(4,2)$ and $M_t(5,1)$) become inaccurate, the identified value of m_z is lower than the nominal value, and m_x and m_y and I_{xx} and I_{yy} are not equal in the identified inertial matrix. Hence, dry friction must be regarded when the dynamic parameters of the real parallel manipulator are identified. In this situation, a modified identification coupling parameter of $27.75 \text{ kg}\cdot\text{m}$ can be obtained using the modified formula proposed in this paper. Comparing with the identified values identified using the Modified Method A and the nominal values which are obtained from analytic formula, it is

found that (1) For mass parameters of inertial matrix $\delta m_x; m_y; m_z$, the maximum identification error is 6.3 kg, 2.3%. (2) For inertial parameters of inertial matrix $\delta I_{xx}; I_{yy}; I_{zz}$, the maximum identification error is 1.6 kg·m², 6.4%. (3) For the cross terms (Mt (1,5), Mt (2,4), Mt (4,2) and Mt (5,1)), the identification error is 12.52 kg·m, 82%. By analyzing the error of data between analytic formula and experiments result, we found that the identification error increases with inertial effects increasing caused by the actuators in identified inertial values. Especially for the cross terms, the max identification error is 82%, which is much larger than the identification error of mass and inertial parameters of inertial matrix. The essential reason is the uncertainty on the dynamic parameters of actuators $\delta i_a; i_b; m_a; m_b; r_a; r_b$ between CAD model and experimental platform. The nonlinear friction effect on dynamic-parameter identification will be further studied in future work This paper takes into consideration multiple influential factors of the measurement accuracy of the interaction forces between components. Among the forces, gravity is of great research interest, and for the first time, this paper provides an analytical algorithm of a six-dimensional F/T with dynamic gravity compensation. The setup of the paper is as follows: Section 1 introduces the digital flexible assembly system and its significance, highlights the applications of the SP, and provides a new perspective and novel methods of large components alignment. Section 2 provides the analytical algorithm of a six-dimensional F/T, proposes a dynamic gravity compensation model based on the screw theory, and offers a parameter which is optimized through experiments. For the spatial precision analysis, Section 3 uses an approximate cone shape to evaluate the accuracy and repeatability of the sixdimensional F/T. In Section 4, using the designed P&O adjusting platform to verify the accuracy of the proposed algorithm and

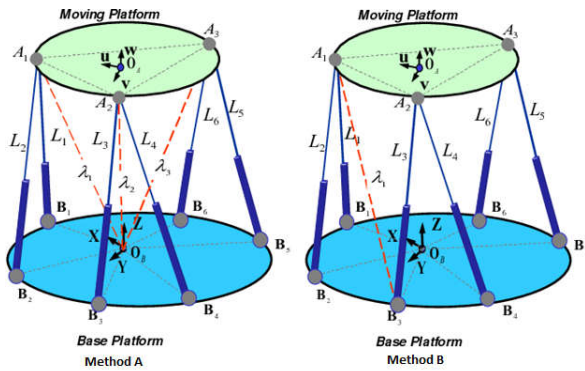
perform spatial precision experiments, relevant experimental data are analyzed and discussed. Section 5 concludes the paper and assesses the validity and limitations of the present algorithm and model.



Method B

The estimated inertial matrix is given in Table , where the identified values of Method A, Modified Method A and Method B are obtained from the experiment, and the nominal value of inertial matrix Mt is obtained from analytic formula. The inertial matrix becomes almost diagonal owing to the platform’s main axes of inertia being set along the platform frame axes, and the cross term m_{qz} (Mt (1,5), Mt (2,4), Mt (4,2) and Mt (5,1)) results from the center of gravity not coinciding with the origin of the moving body frame. In principle, the nominal inertial matrix should be symmetric, which means $Mt (1,5) = Mt (5,1) = m_{qz}$, $Mt (2,4) = Mt (4,2) =$

m_{qz} and $m_z > m_x \frac{1}{4} m_y; I_{zz} > I_{xx} \frac{1}{4} I_{yy}$ when the inertial effects of all the actuators are considered. The difference between the nominal inertial matrix and identified inertial matrix can give some impression of the errors resulting from nonlinear terms. The difference between m_x and m_y is 2 kg when employing Method A but 6.6 kg when employing Method B.



However, for force signals, nonlinear terms are more complex than those in the simulation. Higher harmonic signal components are caused by not only the Coriolis–centrifugal force and dry friction but also a pressure jump in the commutation of the asymmetric hydraulic cylinder²⁵ and the dynamics of the long-stroke hydraulic pipeline that we do not considered in the simulation model.

Then the inertial matrix M_i can be written as

$$M_i = \begin{bmatrix} m_x & 0 & 0 & 0 & -m_{yz} & 0 \\ 0 & m_y & 0 & m_{yz} & 0 & 0 \\ 0 & 0 & m_z & 0 & 0 & 0 \\ 0 & m_{yz} & 0 & I_{xx} & 0 & 0 \\ -m_{yz} & 0 & 0 & 0 & I_{yy} & 0 \\ 0 & 0 & 0 & 0 & 0 & I_{zz} \end{bmatrix} \quad (A9)$$

where

$$\begin{aligned} m_x &= m_y = m + 3(m_w(1 - l_{w1z}^2) + m_{mag}(1 + l_{w1z}^2)), \\ m_z &= m + 6(m_w l_{w1z}^2 + m_{mag}(1 - l_{w1z}^2)), \\ I_{xx} &= I_{cwx} + 3(m_{mag}(a_{1x}^2 + a_{1y}^2 + 2a_{1z}^2 - (v_{1y}^2 + v_{1z}^2)) \\ &\quad + m_w(v_{1x}^2 + v_{1y}^2)), \\ I_{yy} &= I_{cwy} + 3(m_{mag}(a_{1x}^2 + a_{1y}^2 + 2a_{1z}^2 - (v_{1y}^2 + v_{1z}^2)) \\ &\quad + m_w(v_{1x}^2 + v_{1y}^2)), \\ I_{zz} &= I_{cwz} + 6(m_{mag}(a_{1x}^2 + a_{1y}^2 - v_{1z}^2) + m_w v_{1z}^2), \\ m_{yz} &= 3(m_{mag}(l_{w1x}v_{1y} - l_{w1y}v_{1x} - 2a_{1z}) - m_w(l_{w1x}v_{1y} - l_{w1y}v_{1x})). \end{aligned}$$

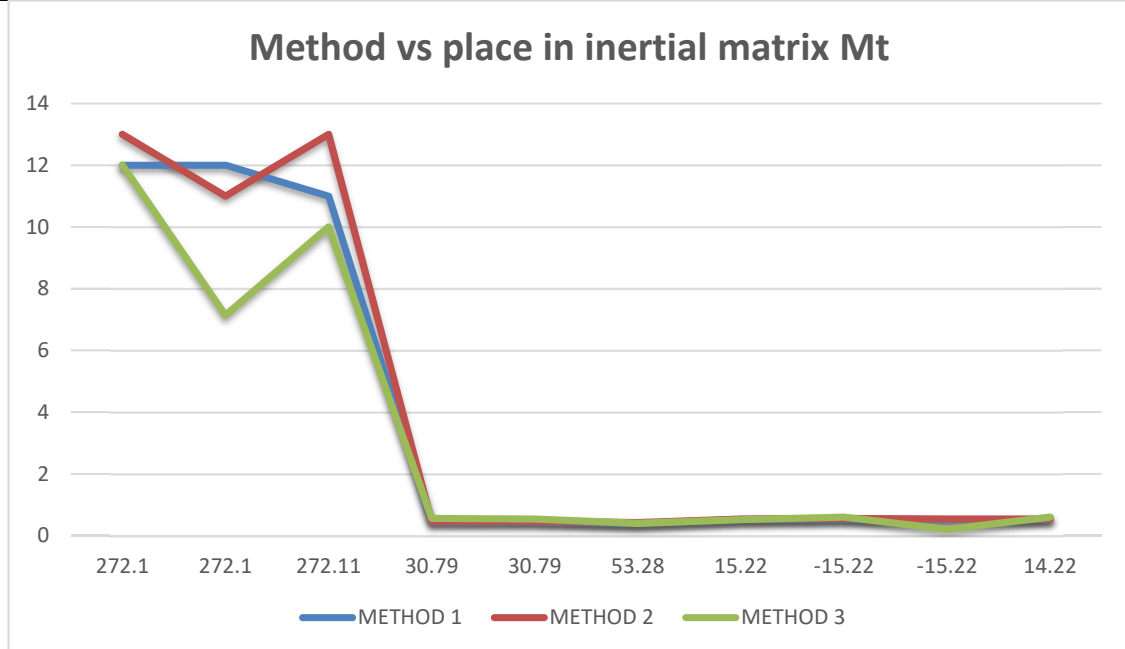
4. Optimization design result analysis of dual-degree-of-freedom magnetic levitation vibration energy harvester

Considering that the acceleration range of bridge vibration brought by vehicles is 0.5 m/s² -1.5 m/s², the excitation amplitude generated by simple harmonic vibration should be set to 1

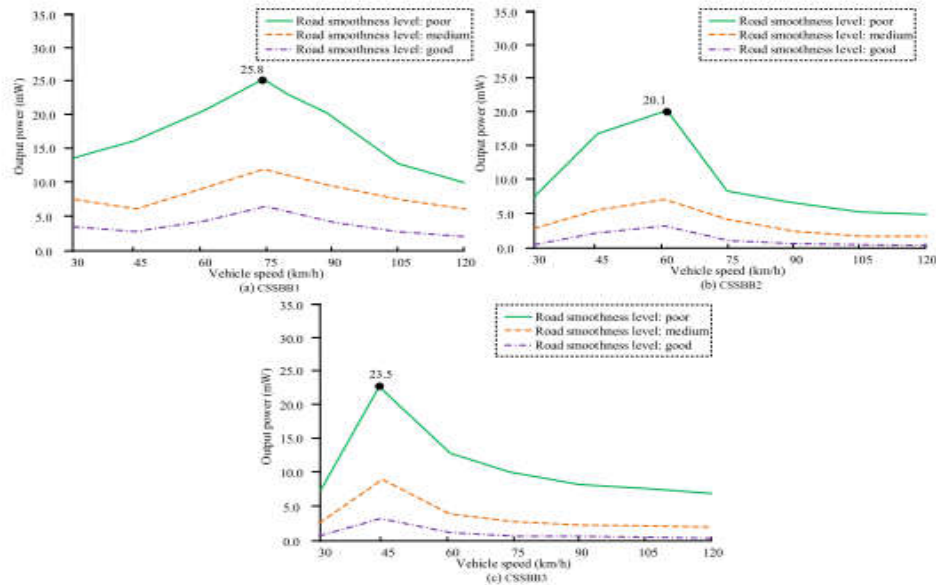
m/s². Combined with the application experience of NSGA-II algorithm in the industry and the characteristics of this axle vibration data, after several debugging, the target parameters, design variables, constraints, population size, number of iteration steps, the crossover coefficient, and the coefficient of variation in NSGA-II algorithm are taken as 2, 9, 2, 100, 200, 0.8, and 0.4, respectively. To increase the comparative value of the study, the SMEH is now used to construct a comparative parameter optimization model according to the same algorithm. The parameters of the SMEH optimization design model are selected in the same way as those of the DMEH. Three concrete simply supported girder bridges of different sizes were selected for the study to assist the optimized design of the vibration energy harvester, and to simplify the description, the abbreviations CSSBB1, CSSBB2, and CSSBB3 were given, and the basic information of the three simply supported girder bridges is shown in Table 1. In addition, each type of simply supported girder bridge. The mathematical models of NSGA-II algorithm, SMEH and DMEH are written in Python language, and the data of the optimal solution set after the optimization of each model is completed are counted to obtain. respectively show the Pareto optimal solution set distribution of simply supported beam bridges CSSBB1, CSSBB2, and CSSBB3 using two vibration energy harvesting models: DMEH and SMEH. The horizontal and vertical axes in Fig. 6 show the negative number of the probability in the maximum output and the total volume of the minimum magnet, respectively, and the icons of different colors represent different energy harvester models. Analysis of Fig. 6 shows that after both models have completed the optimization calculation

PARAMETER	METHOD A	METHOD B	METHOD C	NOMI	PLACE
-----------	----------	----------	----------	------	-------

R	IDENTIFIED VALUE	ERROR (%)	IDENTIFIED VALUE	ERROR (%)	IDENTIFIED VALUE	ERROR (%)	NAL VALU E	IN INERTIAL MATRIX Mt
Mx(kg)	272.42	012	271.42	013	252.72	12	272.10	(1,1)
My(kg)	272.42	012	272.42	011	252.62	7.14	272.10	(2,2)
Mz(kg)	272.42	011	271.42	013	272.45	10	272.11	(3,3)
Ixx(kg.m ²)	30.65	0.45	31.65	0.46	23.41	0.56	30.79	(4,4)
Iyy(kg.m ²)	30.65	0.45	33.65	0.47	23.42	0.54	30.79	(5,5)
Izz(kg.m ²)	53.49	0.40	55.49	0.42	54.49	0.4	53.28	(6,6)
Mt(1,5)(kg.m)	15.30	0.53	14.30	0.54	11.21	0.52	15.22	(1,5)
Mt(2,4)(kg.m)	-15.30	0.54	-14.30	0.56	-11.12	0.6	-15.22	(2,4)
Mt(4,2)(kg.m)	-14.30	0.53	-13.30	0.54	22.03	0.2	-15.22	(4,2)
Mt(5,1)(kg.m)	14.30	0.53	12.30	0.54	-22.03	0.6	14.22	(5,1)



Methods Vs Error (%)



Comparison of total output power of SMEH under different road surface roughness conditions.

A compact identification process that allows estimation of the relevant dynamic parameters of the six-DOF parallel manipulator through identifying a $(6 \cdot 6)$ inertial matrix from the results of six persistently exciting periodic motion tests is proposed in this paper. By solving linear equations based on the ground harmonic of sinusoidal vibrations, velocity-related (friction) and higher order terms (nonlinearities) have minimal effect on the procedure. The proposed identification procedure is validated initially by considering a simulated parallel manipulator for which linear and nonlinear friction models are applied to passive and active joints, respectively. The obtained results show that the new identification procedure is able to handle the coupling phase shift associated with the cross term of viscous friction and can tolerate dry friction using a modified formula with a simple coupling parameter. An experiment is carried out to identify the dynamic parameters of an actual manipulator of this structure. The effect of nonlinear friction in parameter identification is

demonstrated by comparing an inertial matrix obtained from experimental results and a nonlinear friction simulation model. In particular, the proposed identification process can be applied to any parallel manipulator or closed-link mechanism.

5. Conclusion

In conclusion, the integration of a Stewart platform into ambulance stretchers represents a significant advancement in patient transportation technology. By addressing the limitations of conventional stretchers, this system effectively reduces vibrations and enhances patient stability, thereby promoting comfort and safety. The design's adaptability and precision provide a robust foundation for further innovations in medical transport systems.

The results of this study demonstrate the feasibility of employing Stewart platforms for vibration isolation in emergency medical settings. Future work can explore optimization techniques, miniaturization, and cost-effective implementations to make the technology widely accessible. Ultimately, this research highlights the potential to transform patient care during

transit, aligning engineering advancements with critical healthcare needs.

The experimental results show that the maximum total output power of DMEH and SMEH on CSSBB1, CSSBB2 and CSSBB3 are 48.7 mW, 36.8 mW, 25.4 mW and 27.2 mW, 21.5 mW, 14.9 mW, respectively, and the minimum total magnet volumes of both on CSSBB1, CSSBB2 and CSSBB3 are 268 cm³, 132 cm³, 219 cm³ and 214 cm³, 86.2 cm³, 156 cm³. The maximum total output power and corresponding driving speed of DMEH on CSSBB1, CSSBB2 and CSSBB3 are 31.2 mW, 28.9 mW, 31.5 mW and 75 km/h, 60 km/h and 45 km/h respectively. SMEH The maximum total output power and corresponding driving speed on CSSBB1, CSSBB2 and CSSBB3 are 25.8 mW, 20.1 mW, 23.5 mW with 75 km/h, 60 km/h, 45 km/h. The total output power of DMEH is greater than SMEH under various road leveling conditions. When the road leveling is "poor", the maximum total output power of DMEH is 6.0 mW, 8.8 mW and 8.0 mW higher than that of SMEH, respectively. On the whole, if ignoring the vehicle driving speed, the variation of total output power of DMEH is larger than that of SMEH, and the median, maximum and minimum values are larger than that of SMEH. Specifically, the median total power output of DMEH and SMEH under the conditions of "good", "medium" and "poor" road leveling are 4.7 mW, 10.1 mW, 18.5 mW and 10.1 mW, respectively, From the experimental data, it can be seen that the maximum output power of the optimal solution of DMEH is significantly larger than that of SMEH for the selected simply supported girder bridge project, and the volume of the former is larger than that of the latter, but the degree of increase can still be adapted to the application environment

References

- [1] Z. Zhang, J. Sun, L. Wang, J.J. Wei, Multiphysics-coupled study of wind load effects on optical performance of parabolic trough collector, *Sol. Energy* 207 (2020) 1078–1087.
- [2] C. Zhu, J. Yang, C. Rudd, Vibration transmission and energy flow analysis of L-shaped laminated composite structure based on a substructure method, *ThinWalled Struct.* 169 (2021), 108375.1-108375.20.
- [3] Z. Zhu, Z. Wang, K. Dai, X.F. Wang, H. Zhang, W.L. Zhang, An adaptive and space-energy efficiency vibration absorber system using a self-sensing and tunable magnetorheological elastomer, *Nano Energy* 117 (2023) 108927.
- [4] P. Han, G. Pan, B. Zhang, W. Wang, W. Tian, Three-cylinder oscillator under flow: flow induced vibration and energy harvesting, *Ocean Eng.* 211 (2020), 107619.1-107619.17.
- [5] S. Shaaban, Enhancement of the solar trough collector efficiency by optimizing the reflecting mirror profile, *Renew. Energy* 176 (2021) 40–49.
- [6] M. Zhang, C. Zhang, A. Abdelkefi, H. Yu, O. Gaidai, X. Qin, H. Zhu, J. Wang, Piezoelectric energy harvesting from vortex-induced vibration of a circular cylinder: effect of Reynolds number, *Ocean Eng.* 235 (2021), 109378.1-109378.13.
- [7] C. Liu, R. Zhao, K. Yu, H.P. Lee, B. Liao, A quasi-zero-stiffness device capable of vibration isolation and energy harvesting using piezoelectric buckled beams, *Energy* 233 (2021), 121146.1-121146.18.
- [8] E. Masero, J.M. Maestre, E.F. Camacho, Market-based clustering of model predictive controllers for maximizing collected energy by parabolic-trough solar collector fields, *Appl. Energy* 306 (2022), 117936.1-117936.12.
- [9] X. Liu, C. Sun, Y. Wang, F. Jiang, C. Zhang, Vibration characteristic analysis of transformers influenced by DC bias based on vibration half-wave energy method, *Int. J. Electr. Power*

- Energy Syst. 128 (4) (2021), 106725.1-106725.8.
- [10] Z.Q. Lu, D. Wu, H. Ding, L.Q. Chen, Vibration isolation and energy harvesting integrated in a Stewart platform with high static and low dynamic stiffnessScienceDirect, Appl. Math. Model. 89 (Pt. 1) (2021) 249–267.
- [11] H. Zhang, X. Xiang, B. Huang, Z. Wu, H. Chen, Static homotopy response analysis of structure with random variables of arbitrary distributions by minimizing stochastic residual error, Comput. Struct. 288 (2023) 107153.
- [12] J. Wang, F. Liang, H. Zhou, M. Yang, Q. Wang, Analysis of position, pose and force decoupling characteristics of a 4-ups/1-rps parallel grinding robot, Symmetry 14 (4) (2022) 825.
- [13] K. Liao, D. Lu, M. Wang, J. Yang, A low-pass virtual filter for output power smoothing of wind energy conversion systems, IEEE Trans. Ind. Electron. 69 (12) (2022) 12874–12885.
- [14] M. Chen, X. Zhang, J. Liu, F. Liu, R. Zhang, P. Wei, H. Feng, M. Tu, A. Qin, W.Y. Lam, D. Ding, B.Z. Tang, Evoking photothermy by capturing intramolecular bond stretching vibration-induced dark-state energy, ACS Nano 14 (4) (2020) 4265–4275.
- [15] J. Wang, L. Tang, L. Zhao, G. Hu, R. Song, K. Xu, Equivalent circuit representation of a vortex-induced vibration-based energy harvester using a semi-empirical lumped parameter approach, Int. J. Energy Res. 44 (6) (2020) 4516–4528.
- [16] Q. Cai, S. Zhu, The nexus between vibration-based energy harvesting and structural vibration control: a comprehensive review, Renew. Sustain. Energy Rev. 155(2022), 111920.1-111920.24.
- [17] J. Ke, J. Gao, Z.Y. Wu, Z. Xiang, X.D. Hu, Vari-stiffness characteristics of a 3D SMA hybrid basalt woven composite, Compos. Struct. 285 (2022), 115192.1- 115192.14.